J. Fluid Mech. (2001), *vol.* 432, *pp.* 201–217. Printed in the United Kingdom

© 2001 Cambridge University Press

Diffusion-controlled solidification of a ternary melt from a cooled boundary

By ANNELI AITTA, HERBERT E. HUPPERT AND M. GRAE WORSTER

Institute of Theoretical Geophysics, Department of Applied Mathematics and Theoretical Physics, University of Cambridge, Cambridge CB3 9EW, UK

(Received 6 April 2000 and in revised form 25 September 2000)

We present details of an experimental study of crystallization adjacent to a cooled boundary from an aqueous solution of potassium nitrate and sodium nitrate. This transparent system is typical of many ternary melts that do not form solid solutions, including examples in igneous petrology and metallurgy. We have measured the rates of advance of the front of crystallization and the eutectic front, behind which the system is completely solid. From careful measurements of the concentration and temperature fields, we have been able to infer the location of an internal phase boundary: the cotectic front separating a region in which only one component of the ternary system forms crystals from a region in which two components form crystals. Our experiments were conducted under conditions in which fluid flow is minimal, so that rates of crystallization are determined principally by the diffusive transport of heat. We have confirmed that the thicknesses of the various regions all grow in proportion to the square root of time, as is expected of diffusion-limited growth, and have determined the constants of proportionality for a range of different initial concentrations and boundary temperatures. We have found evidence to suggest that there may be a significant nucleation delay in the secondary and tertiary crystallization. Our measurements of concentration provide much more information about the ternary phase diagram than has hitherto been available.

1. Introduction

The formation of solids by the cooling of liquid melts is a fundamental process in a wide range of industrial and natural settings. Although there are some examples of the solidification of (almost) pure liquids, such as the making of ice cubes in a freezer, most situations involve the solidification of liquids made up of many constituents. Examples include the fabrication of modern super alloys and the solidification of molten lava.

Many fundamental aspects of solidification of multi-component melts can be determined from studies of the solidification of binary, or two-component, melts. For example, they explain how a component of the melt can be preferentially incorporated into the solid phase, causing the melt to become enriched in its other components. Such enrichment results in local constitutional supercooling (Tiller *et al.* 1953); the melt adjacent to the front of solidification finds itself at a temperature below its equilibrium freezing temperature, owing to the variation of freezing temperature with the composition of the melt. This can result in an instability of the phase boundary (Mullins & Sekerka 1964) and the formation of a mushy layer in which the solid

https://doi.org/10.1017/S0022112000003232 Published online by Cambridge University Press

forms a porous matrix of crystals bathed in residual liquid (see Worster 1992 for a review). Though solidification can be made to occur at a stable, planar front with careful control of the solidification rate, it is much more common in castings and natural settings for solidification of multi-component melts to occur through the formation of mushy layers. Solute enrichment also results in density gradients that can drive various interacting types of compositional and thermal convection (Huppert & Worster 1985; Huppert 1990). Even more complex behaviour can occur in multi-component melts when, for example, density inversions occur as each component of the melt is sequentially solidified.

Some generally observed phenomena cannot be explained in terms of binary systems but can, at least partially, be understood in terms of ternary, or three-component, systems. Indeed geologists, who study arguably the most complex multi-component materials on Earth in the form of multi-mineralic rocks, often try to capture the essence of observed phenomena by considering crystallization sequences in terms of three major constituents; for example, the formation of granite in terms of quartz, mica and feldspar. In one of the few studies of convection and solidification in ternary systems, Huppert & Sparks (1980) put forward an explanation of the formation of Mid-Ocean-Ridge Basalts (MORBs) in terms of the sequence olivine–plagioclase–pyroxene in which an important part is the fact that the density of the melt first decreases as olivine crystallizes then increases again as plagioclase crystallizes.

In many accounts of fractional crystallization, interpretations are based on equilibrium cooling and crystallization in bulk, plus an assumption that the solid formed at each stage is removed from the system. While this can happen to some extent if crystals of the solid phase are formed in suspension and settle to the floor, it is also common for solidification to proceed from the cooled boundaries of a mould (or magma chamber) and to form a mushy layer from which the residual melt may or may not be able to escape by compositional convection (Wettlaufer, Worster & Huppert 1997). Then, there is not only a temporal evolution of the composition of the melt but also spatial variations of its composition and of the fraction of solid formed.

In this paper, we commence a systematic study of solidification of ternary melts resulting from cooling at a boundary. We have conducted a series of laboratory experiments using an aqueous solution of two salts: sodium nitrate and potassium nitrate. In this initial study we cooled the melt from a lower, horizontal boundary and confined the experiments to the region of the phase diagram in which the density of the residual melt progressively increased as crystallization proceeded. Thus there was minimal convection in the system, neither thermal nor compositional.† Our approach here mirrors that which we adopted to study two-component systems, for which Huppert & Worster (1985) identified a 3×2 table of possibilities, most involving convection. However, they initially investigated only the situation in which thermal and compositional convection were absent. Since then all six cases have been investigated, and a general discussion of our current state of understanding can be found in Worster (2000). In this paper we present our detailed measurements of the time evolution of the temperature and compositional fields as well as the rates of solidification. In doing so, we have charted features of the ternary phase diagram and determined the extent to which local equilibrium is maintained within the evolving system.

† Lateral temperature gradients due to thermal leakage through the sidewalls of a mould may occur and cause some extraneous convection, but its influence is weak and will not be considered here.

https://doi.org/10.1017/S0022112000003232 Published online by Cambridge University Press

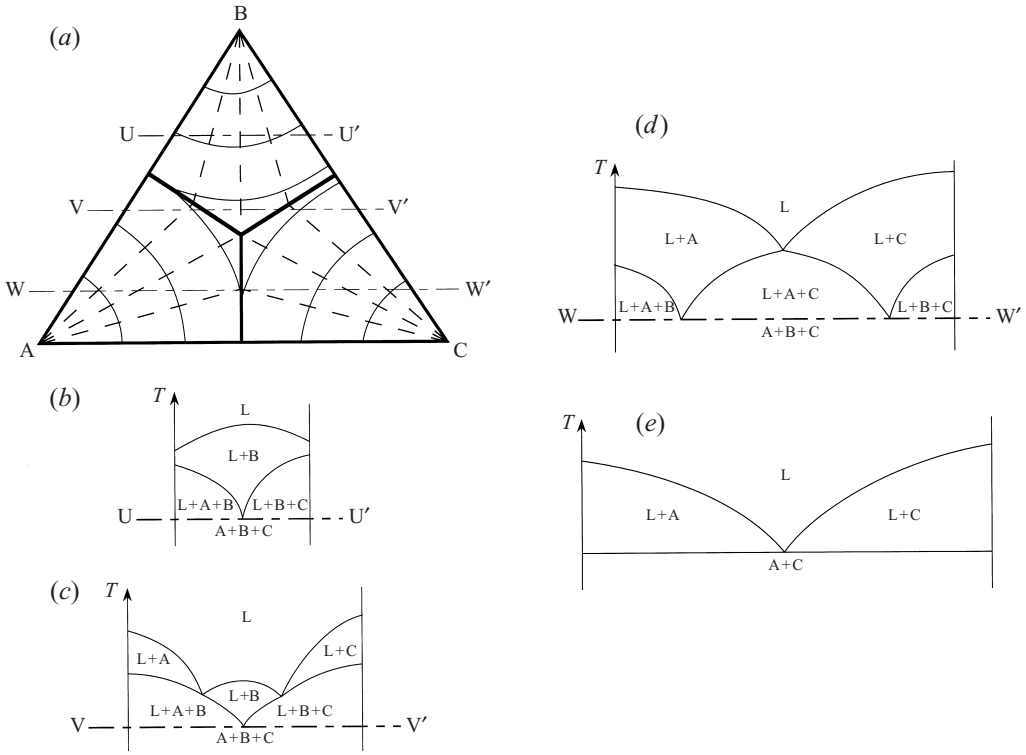


FIGURE 1. (*a*) Plan view of a simple, ternary phase diagram for components A, B, C that produce pure crystals, with no solid solutions. The thick lines (cotectics) separate the *fields* of the respective components. The thinner, solid lines are temperature contours on the liquidus surfaces, while the dashed lines are temperature contours on the solidus surfaces. (*b–d*) Vertical cross-sections, as indicated by horizontal, long/short dashed lines in (*a*), giving the phases (liquid L and solids A, B and C) present in equilibrium at a given temperature and bulk composition. (*e*) The binary phase diagram, which applies along the AC-axis.

We begin in § 2 with a description of a typical ternary phase diagram and a description of the spatial and temporal sequences of crystallization that should occur during solidification. These serve as a guide and basis for comparison for our experimental observations and measurements. The experimental method and the measurement techniques used are described in § 3. Results are presented in § 4 and discussed in § 5.

2. A ternary phase diagram

The phase diagram for a chemical system identifies the solid and liquid phases that are present in thermodynamic equilibrium when a sample of a given overall composition is held at a given temperature. A schematic phase diagram for a two-component system and its simplification for a typical aqueous solution is discussed in Worster (2000). It forms one section of the phase diagram of a ternary system, as described below in reference to figure 1(*e*). The phase diagram of a ternary system (West 1982) is three-dimensional and therefore difficult to represent in detail in a single, planar figure. We shall consider the simplest cases pertinent to aqueous solutions in which the only crystals that form consist purely of one of the three constituents.

https://doi.org/10.1017/S0022112000003232 Published online by Cambridge University Press

A schematic plan of such a phase diagram is shown in figure 1(*a*). This figure is idealized in being almost symmetric with respect to the three components; in reality, such symmetry is unusual, but this aspect is not important in any of the phenomena described in this paper. The phase diagram represents the composition of the system in terms of a non-orthogonal basis in which the axes indicate the mass fraction (in weight percent) of two solutes (salts) B and C dissolved in a third solvent (water) A. Three cotectic curves, shown as thick lines, separate the space into three regions, one associated with each vertex of the diagram, called the *field* of the respective component. Also shown on the diagram are two sets of temperature contours. The first set, shown with solid curves, is the *saturation curves*, which indicate the concentrations of saturated solutions at the given temperature. These are the contours of the *liquidus surface* at which solid can first form as the liquid is cooled. The first crystals to form are those corresponding to the field in which the overall (bulk) composition of the liquid resides. The second set of contours, shown with dashed lines, gives values of the temperature at which a second crystal begins to form. The crystallization sequence that occurs as a sample of given overall composition is cooled can be seen from the cross-sections shown in figure 1(*b–d*). We see that, depending on where one starts in the phase diagram, a variety of sequences of crystallization can occur. This three-dimensional phase diagram is an extension of the simple binary-eutectic phase diagram shown in figure 1(*e*), which applies along the AC-axis. The cross-sections in figure 1(*b–d*) cannot be interpreted as two-component phase diagrams to infer liquid compositions, which must be deduced from the full three-dimensional figure as follows.

A common way to use the phase diagram is to trace out the *liquid line of descent*, which shows the evolution of the residual liquid as crystallization proceeds. An example is shown in figure 2. A liquid of initial composition O forms crystals of pure component A on first reaching the liquidus, as shown on the left-hand side of figure 1(*c*). The composition of the residual liquid therefore evolves along the straight line, the *tie line*, through A and O until it reaches the cotectic curve at P. The cotectic curve is the extension of the binary eutectic point E_{AB}. On further cooling, crystals of pure component B are formed in addition to those of A, and the composition of the residual liquid evolves along the cotectic curve until reaching the eutectic point E. Further cooling results in the crystallization of all three components to form a composite solid with no liquid remaining. While evolving along the cotectic curve, the proportion of A and B crystals is determined by constructing the tangent to the curve, as shown in figure 2 and finding its intercept on the AB-axis.

The phase diagram can be used to determine the expected structure of crystallization at a cooled boundary if the system evolves through states that are in local equilibrium. This is shown schematically in figure 3. The temperature increases continuously away from the cooled boundary. In the warmest region ($z > h$, $T > T_0$) the system is completely liquid. At temperatures below T_0 (the saturation temperature corresponding to the initial concentration of the liquid) a mushy layer forms, consisting initially of crystals of component A bathed in a melt enriched in both components B and C.

Below $z = h_c$, the height at which the residual liquid reaches the cotectic curve (point P in figure 2) at temperature T_P, there is a *cotectic mushy layer* in which the solid matrix is composed of crystals of both A and B. The residual melt therefore continues to be enriched in component C but may become depleted of component B. Finally, below $z = h_E$ the height at which the eutectic temperature T_E is reached, the system is completely solid in the form of a composite of crystals of all three components.

https://doi.org/10.1017/S0022112000003232 Published online by Cambridge University Press

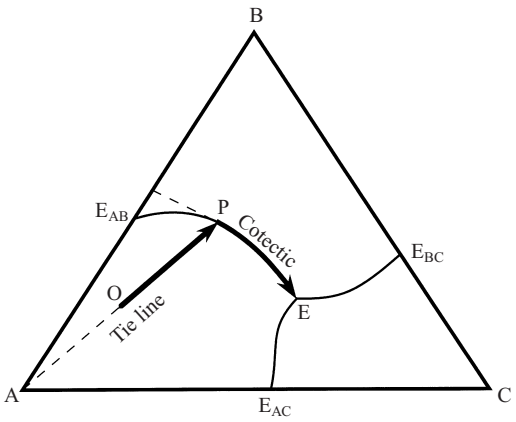


FIGURE 2. The liquid line of descent. OPE shows the evolution of the composition of the residual liquid as a melt of initial composition O is progressively solidified.

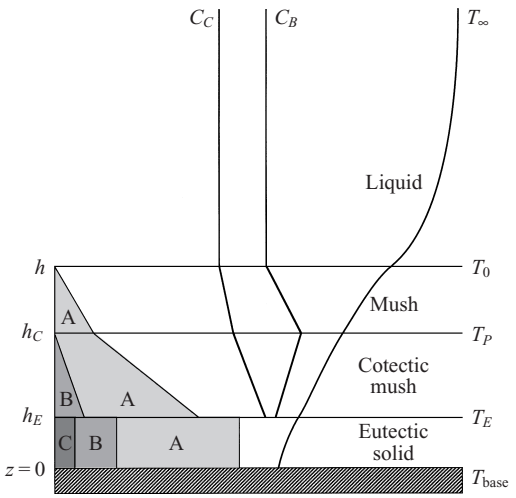


FIGURE 3. Schematic diagram of solidification from a cooled boundary. If the temperature of the boundary is below the three-phase eutectic temperature then three distinct layers form, as shown. The shaded regions on the left indicate the relative proportion of each of the solid phases present at each height. The two concentration curves, C_B and C_C, indicate the concentrations of components B and C dissolved in solvent A in the residual liquid of each height. On the right are shown the temperatures T_0, T_P, T_E and T_{base} corresponding respectively to the interface and boundary positions h, h_C, h_E and $z = 0$.

This would be the picture if local equilibrium prevailed at all stages. We shall see that in the experiments we conducted, significant disequilibrium was encountered. In our experience, thermal disequilibrium is quite common in many crystallization situations. Disequilibrium during solidification can have a significant influence on the strength and nature of convection in the system. In combination, disequilibrium and convection of the liquid region has been shown to cause additional crystallization in regions remote from the cooled boundary (Kerr *et al.* 1990) and can suppress the convection internal to the mushy region that can result in the formation of channels of reduced solid fraction called chimneys (Worster & Kerr 1994).

https://doi.org/10.1017/S0022112000003232 Published online by Cambridge University Press

The changes in composition of the residual liquid cause its density to change, and this may lead to buoyancy-driven convection. For the case in which the system is cooled from a lower, horizontal boundary there is no thermal convection. However, depending on how the density of the liquid varies with concentration, the mushy layer and the cotectic mushy layer can jointly or severally be prone to compositional convection. Various sandwiches of stability can be formed each, no doubt, with its own characteristics.

In the present study, we investigate the simplest situation in which the density of the residual liquid increases along the whole line of descent, so that there is no convection expected. In such circumstances, solidification is governed entirely by diffusion and by the kinetics of nucleation and growth. Further, the rate of growth of a mushy layer is controlled principally by the rate of thermal diffusion and is not limited by the slower rate of solutal diffusion (Huppert & Worster 1985; Worster 1986; and see review by Worster 2000).

3. Experimental method

A significant time was spent determining a suitable ternary system for use in the laboratory. Our criteria were: that the liquid should be transparent, so that we could make visual observations of the evolving system; that the phase diagram be simple (other aqueous salt solutions we considered form double salts, some quite close to the eutectic point), so that the experiments would conform as closely as possible to the simplest theories that might be developed; that the liquidus and eutectic temperatures be not too far distant from room temperature, so that we could achieve solidification with relatively simple apparatus; and that concentrations of the liquid should be readily and accurately measurable. These considerations led us to the system of potassium nitrate (KNO_3) and sodium nitrate ($NaNO_3$) dissolved in water. This system has a eutectic temperature of $-19.0\,^{\circ}C$ and the individual proportions of the two salts can be accurately determined by measuring the concentration of potassium and sodium ions using atomic absorption spectroscopy.

3.1. *The phase diagram*

We were able to find very little published data on the phase diagram. There are a number of published saturation curves for temperatures above $0\,^{\circ}C$ but almost no data in the ice field. Those data that we were able to find are presented in figure 4. They are sufficient to give an approximate indication of the cotectic between KNO_3 and $NaNO_3$ but not the other two cotectics. The experiments reported in this paper all have initial concentrations in the ice field. The only relevant published data are the two binary eutectic points (E_{AB} and E_{AC}) and the three-phase eutectic point E. The dot-dashed lines are simply the straight lines joining these points and give a preliminary indication of the location of the cotectic curves.

3.2. *The apparatus*

The experimental investigations were conducted by filling a tall rectangular Perspex tank, of internal horizontal dimensions 20 cm × 20 cm and walls 1.3 cm thick, with solution to a depth of about 33 cm. The tank was insulated with a 5 cm thick layer of expanded polystyrene around the sidewalls and a 10 cm thick layer above and below the tank. The base of the tank was a 2.5 cm thick brass plate within which cooled ethylene glycol (mixed 50% with water) was pumped through a double-spiral channel.

https://doi.org/10.1017/S0022112000003232 Published online by Cambridge University Press

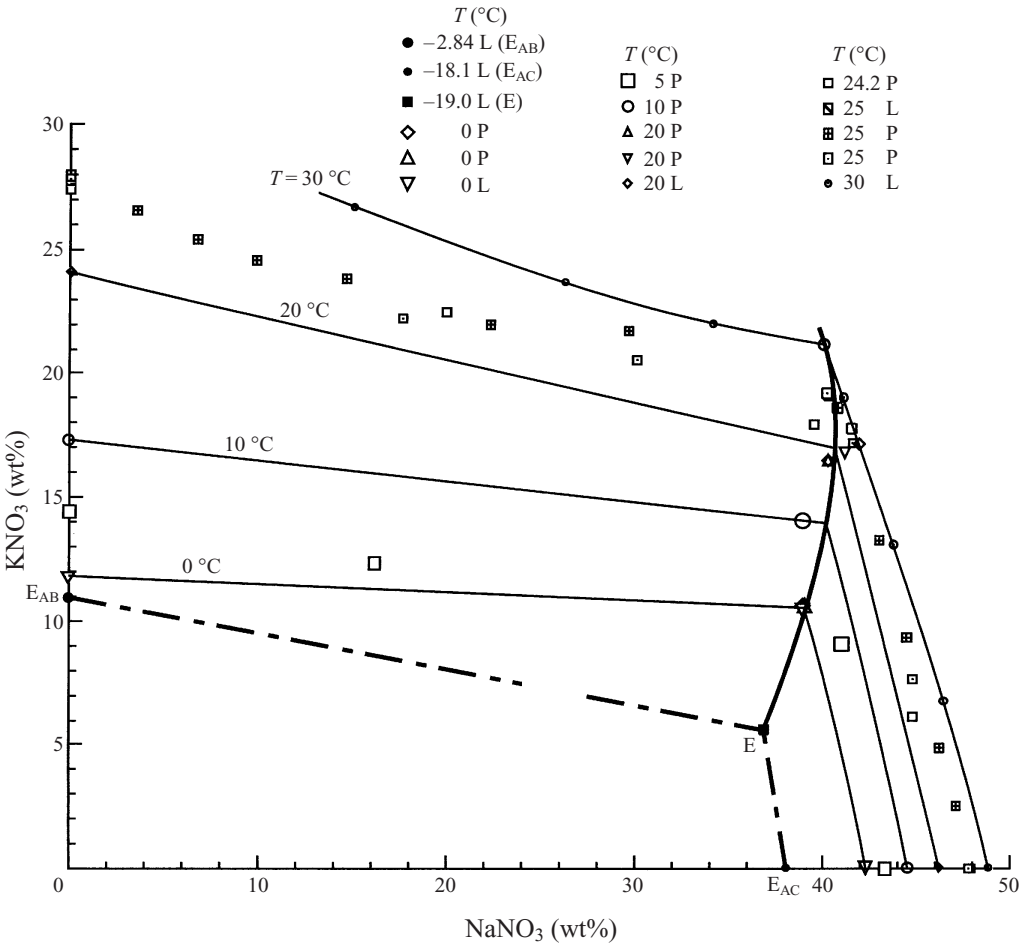


FIGURE 4. The phase diagram for H_2O–KNO_3–$NaNO_3$. The solubility data, indicated by different symbols, are from Linke (1965) (L) and Protsenko *et al.* (1971) (P). The thick dot-dashed and solid lines are hand-drawn estimates of the cotectic curves based on the available data (shown by the solid or slightly enlarged symbols). Note that the phase diagram is presented using orthogonal coordinates.

Temperatures were measured using glass-bead thermistors connected to a computer via a bridge and an A to D board. One thermistor was embedded in the middle of the base, close to its upper surface. Seven other thermistors were positioned at 1, 2.5, 4, 8, 10, 12 and 20 cm above the base, 6 cm from the nearest wall and equidistant from the two second nearest walls. These thermistors were mounted on the ends of hollow stainless steel rods protruding horizontally through sealed holes in the side of the tank. The thermistors were calibrated before each experiment. During an experiment, temperatures were logged automatically by a computer at specified time intervals.

Fluid of the chosen initial concentration was prepared by dissolving commercial salts (with total impurities less than 2%) into deionized tap water that was then filtered. Using a bypass circuit, the coolant was precooled overnight to a temperature of about −29 °C. At the start of each experiment the coolant was redirected to flow through the base plate. During each experiment the thermostat on the cooler was adjusted manually to keep the base temperature (as measured by the thermistor

https://doi.org/10.1017/S0022112000003232 Published online by Cambridge University Press

embedded within it) as constant as possible. Once the desired base temperature was achieved it could be maintained constant to within $\pm 0.1\,^{\circ}\mathrm{C}$.

3.3. *Measurements*

The computer was set to record the temperature every 0.1 min initially and usually every 5 min after the first couple of hours. The duration of the experiments varied from 23 to 120 h. The growth of crystals was monitored visually and the heights of the top of the mushy layer and of the eutectic solid were measured by means of a ruler. The position of the top of the cotectic mushy layer could not be seen, and so could not be measured directly, but was inferred from measurements of the interstitial concentration.

Samples of liquid were withdrawn periodically from several positions in the tank: near the bottom, middle and top of the fully liquid region and every centimetre or so through the mushy layers. The latter samples were obtainable because there was usually some separation between the mush and the walls of the tank.

The salt concentrations of the samples were measured using atomic absorption from flame emission. The samples were first diluted 1:500 by volume in order to reach the working range of the spectrometer. Fluids of known concentrations of each salt were prepared, covering the whole regime of interest, and used to calibrate the output of the spectrometer. The stability of the calibration was checked after approximately every 10 measurements.

The output from the spectrometer gave individual concentrations of Na and K in $\mu\mathrm{g\,cm^{-3}}$. The concentrations of the respective salts ($NaNO_3$ and KNO_3) in volume percent were then determined by multiplying by the dilution factor 500, a factor of 10^4 (to convert from p.p.m. to percent) and the molecular weight of the salt divided by the atomic weight of the respective element. Finally, the concentration in weight percent was determined by dividing by the density of the liquid. We did not measure the density of the samples directly but used the formula for the density ρ of solutions at $20\,^{\circ}\mathrm{C}$:

$$\rho = 1 + a_1 N + b_1 K + a_2 N^2 + b_2 K^2 + cNK,$$

where N and K are the concentrations (wt%) of $NaNO_3$ and KNO_3 respectively, and the coefficients $a_1 = 0.006387$, $a_2 = -6.728 \times 10^{-6}$, $b_1 = 0.005898$ and $b_2 = -2.227 \times 10^{-6}$ were obtained by regression to data for each of the binary salt-water systems at $20\,^{\circ}\mathrm{C}$. The coefficient $c = 2.083 \times 10^{-4}$ of the cross-term was determined from a fit to the median of data at a single concentration given by various authors, namely that $\rho = 1.494\,\mathrm{g\,cm^{-3}}$ at $N = 41.21\,\mathrm{wt\%}$, $K = 16.77\,\mathrm{wt\%}$ and $T = 20\,^{\circ}\mathrm{C}$ (Protsenko, Razumovskaya & Brykova 1971).

4. Observations and results

4.1. *Visual observations*

Crystals formed a few minutes after the coolant began to flow through the base, usually at just one location, and the front of crystallization spread horizontally until the base was covered after about another 30 s. A curiosity of marginal interest in the present study is that the crystallization front progressed across the base of the tank as alternating lighter and darker bands, which might indicate some periodicity in the growth rate and/or the solid fraction of this initial rapid crystallization.

The top surface of the mushy layer was very flat for the first 40 min or so, at which time a thin layer (< 1 mm) of homogeneously distributed, spiky crystals became visible

https://doi.org/10.1017/S0022112000003232 Published online by Cambridge University Press

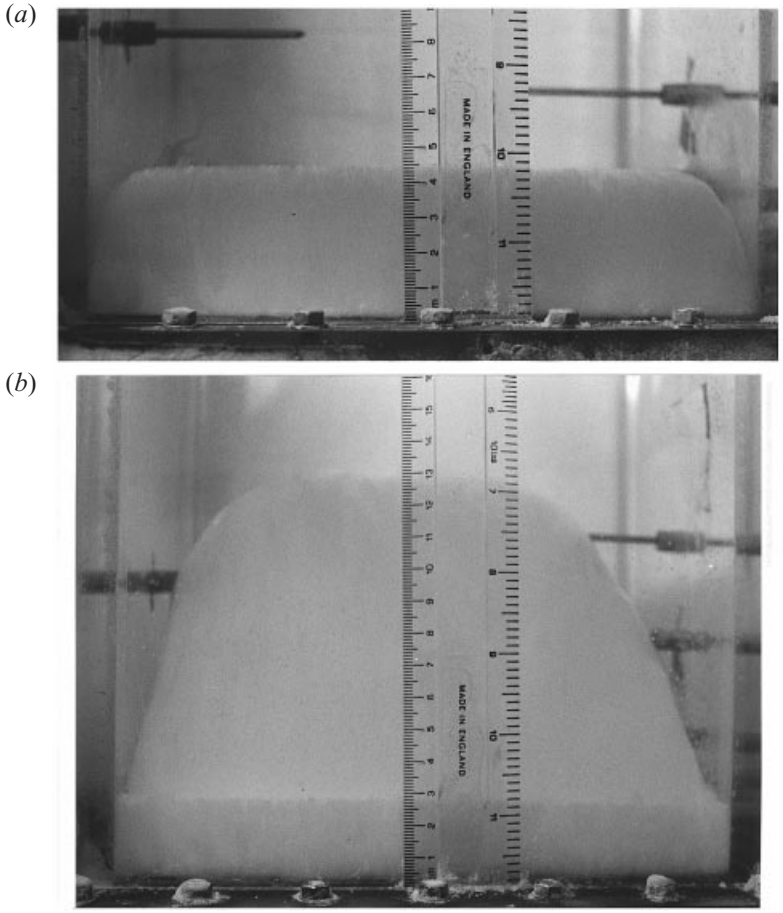


FIGURE 5. Photographs taken from the side during experiment 7. (*a*) After 5.1 h, the top of the mushy layer is at $h = 4.7$ cm, while the euctectic front at $h_E \simeq 0.3$ cm is barely visible. (*b*) After 82.5 h the eutectic front has grown to 2.75 cm and the top of the mushy layer to 14.4 cm. There is a large gap between the mushy layer and the side of the tank at this stage, while the eutectic front extends all the way to the sidewalls.

protruding from the surface. After about 1.2 h, weak patterns in the form of locally aligned, curved, narrow rolls with separation less than 0.5 cm appeared on the surface. Over time they developed, widened and deepened until after about 4 h (figure 5*a*) the surface was quite uneven (on a vertical scale of about 5 mm). At this stage the position of the interface was estimated as the horizontal envelope of the corrugations. By the end of an experiment (figure 5*b*) these surface corrugations had become a major feature consisting of curved, half-cylinders meeting at rather deep (~ 1 cm) indentations.

Owing probably to heat gains from the laboratory but possibly also to interactions between whatever causes the surface corrugations and the sidewalls, the mushy layers became progressively separated from the sidewalls of the tank. The liquid separating the mushy layers from the walls occupied a wedge of zero thickness at its base increasing to about 1 cm when the mushy layer was 4.7 cm high and to a little over 2 cm when the mushy layer was 14.4 cm high (figure 5).

In two of the seven experiments, the base temperature was held below the three-phase eutectic temperature. The three-component eutectic solid was easily observed

https://doi.org/10.1017/S0022112000003232 Published online by Cambridge University Press

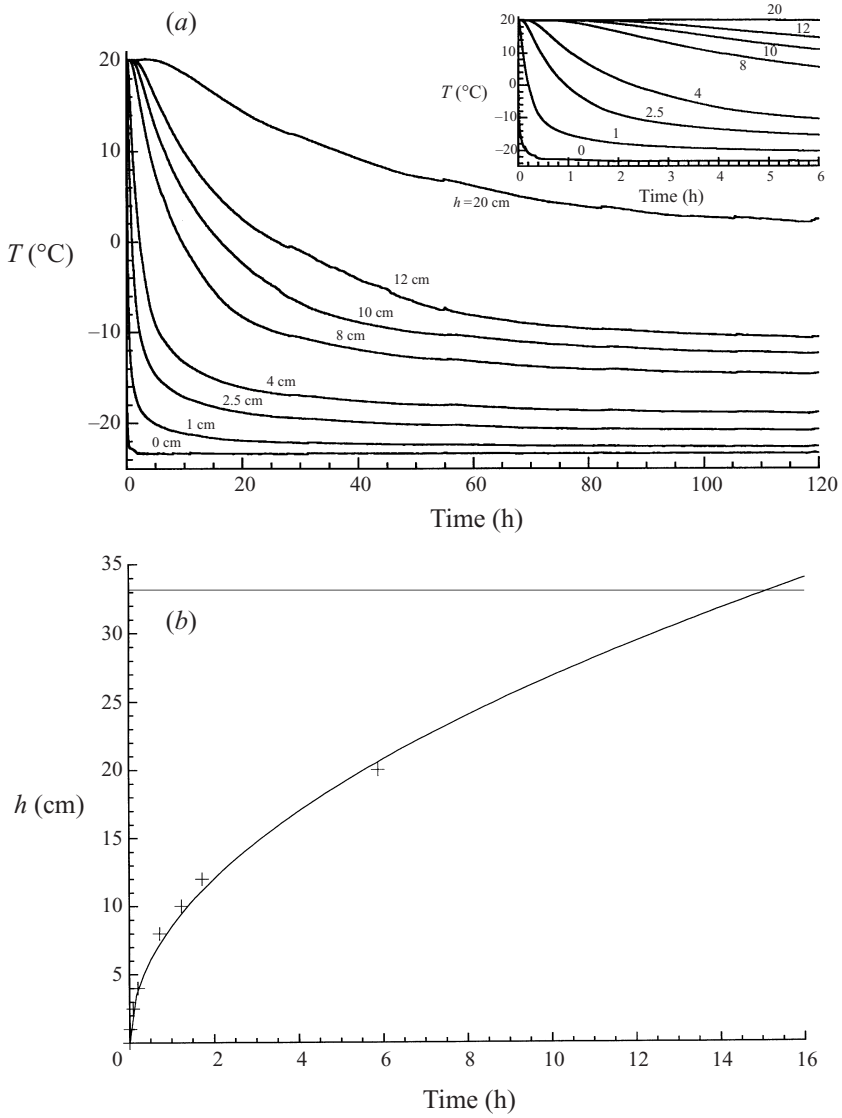


FIGURE 6. (*a*) Temperature as a function of time measured by the fixed thermistors at the indicated heights. The early stage is shown in detail in the insert. (*b*) The thickness of the thermal boundary layer, estimated by recording the time at which the temperature first falls to 0.1 °C below its initial value.

as a bright white region that contrasted with the translucent mushy layers, as visible in figure 5(*b*). The upper surface of the eutectic solid was quite flat, all the way to the edges of the tank.

4.2. *Temperature measurements*

Traces from all eight thermistors during a typical experiment (experiment 7, table 1) are shown in figure 6(*a*). Initially, all thermistors show room temperature. A base temperature of $-22.7\,^{\circ}\mathrm{C}$ was achieved in about 30 min and it took a further hour to reach $-23.35 \pm 0.05\,^{\circ}\mathrm{C}$. In this system, cooling is by conduction alone. The thickness of the diffusive thermal boundary layer can be estimated by recording the times at

https://doi.org/10.1017/S0022112000003232 Published online by Cambridge University Press

Expt.	Initial concentration (wt%) $NaNO_3$	Initial concentration (wt%) KNO_3	a ($cm\,s^{-1/2}$)	a_C ($cm\,s^{-1/2}$)	a_E ($cm\,s^{-1/2}$)	Base temperature (°C)	Fluid height (cm)	Duration (h)
1	9.7	8.0	0.0224			−16.0	31.0	120
2	10.4	3.4	0.0242	0.008		−15.0	31.0	23
3	11.4	5.7	0.0223	0.015		−15.0	31.0	29
4	4.4	8.4	0.0268			−16.0	31.0	53
5	11.9	2.2	0.0315	0.008		−19.7	31.0	25
6	14.6	1.2	0.0378	0.014	0.0110	−27.7	33.2	27
7	15.2	3.5	0.0329	0.011	0.0049	−23.3	33.2	120

TABLE 1. Experimental parameters. a, a_C, and a_E are respectively the constants of proportionality between h and $t^{1/2}$ for the mush–liquid interface, the cotectic front and the eutectic front.

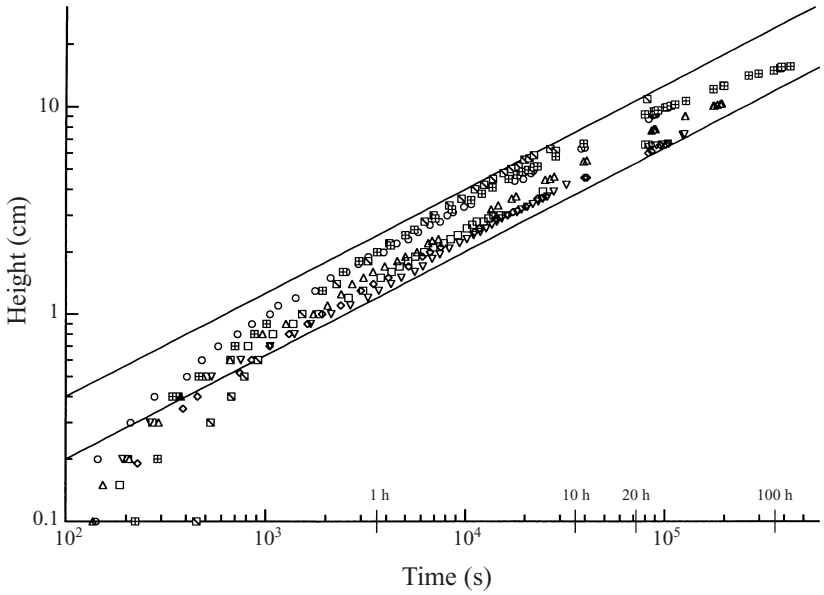


FIGURE 7. The height of the mushy layer as a function of time measured in each of the experiments. The lines are drawn with slopes of 0.5 and coefficients of 0.02 and 0.04 $cm\,s^{-1/2}$.

which each thermistor reached a temperature 0.1 °C below its starting value. This is shown in figure 6(*b*), where we see that the boundary-layer thickness is fitted very well by a curve of the form $h = a_T t^{1/2}$ with $a_T = 0.141\,cm\,s^{-1/2}$. This corresponds to the theoretical result for a medium of thermal diffusivity $\kappa = 1.1 \times 10^{-3}\,cm^2\,s^{-1}$, which compares well with the value $\kappa = 1.35 \times 10^{-3}\,cm^2\,s^{-1}$ for water at 0 °C. This figure also shows that the thermal boundary layer reaches the top of the fluid layer after about 15 h. It can therefore be anticipated that the growth of crystals will be self-similar and proceed at a rate proportional to $t^{1/2}$ for times less than 15 h but that for later times the finite size of the tank will have an influence on their growth.

4.3. *Measured heights*

The height of the mush–liquid interface h for all the experiments is shown in figure 7. We see that for a substantial period, between about 10^3 s and 10^5 s, the heights grow

https://doi.org/10.1017/S0022112000003232 Published online by Cambridge University Press

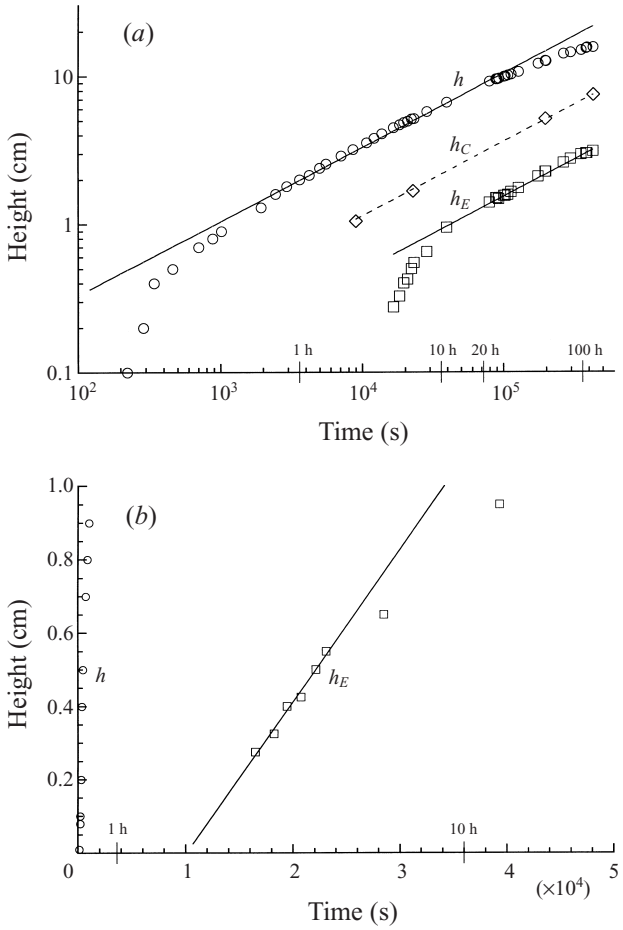


FIGURE 8. (*a*) The heights of the mushy layer h and eutectic front h_E measured directly in experiment 7. The height of the cotectic front h_C is inferred from the concentration measurements shown in figure 9. The lines are the 'best-fit' lines of slope 0.5 through the appropriate part of the data as discussed in the text and reported in table 1. (*b*) Close-up of the data on a linear scale to show the delay and the initial linear growth in time at the eutectic front.

in proportion to $t^{1/2}$. At earlier times (less than about 15 min) the growth deviates from this law owing to the transients associated with the initial cooling of the base plate. At greater times ($> 10^5$ s $\simeq 28$ h) effects due to the finite size of the container play a (weak) role, as discussed above, and the growth again deviates from this law. The constant of proportionality between h and $t^{1/2}$, obtained by the best fit to the data for $10^3\,\mathrm{s} < t < 10^5\,\mathrm{s}$ is given for each experiment in table 1.

The height of the mush–liquid interface h, the cotectic front h_C and the eutectic front h_E measured in experiment 7 are shown in figure 8. Measurement of the mush–liquid interface h has been described above. Composite (eutectic) solid became visible after about 3 h, and its height h_E could be easily measured at the side of the tank using a ruler. We see that its growth is well-fitted by the function $h_E = a_E t^{1/2}$ after about 10 h until the end of the experiment, where $a_E = 4.86 \times 10^{-3}\,\mathrm{cm\,s^{-1/2}}$. Although this is mostly after the time at which the thermal boundary layer reaches the top of the liquid layer, the growth of the eutectic layer is governed principally by a balance between latent heat released at the eutectic front and the heat conducted back to the

https://doi.org/10.1017/S0022112000003232 Published online by Cambridge University Press

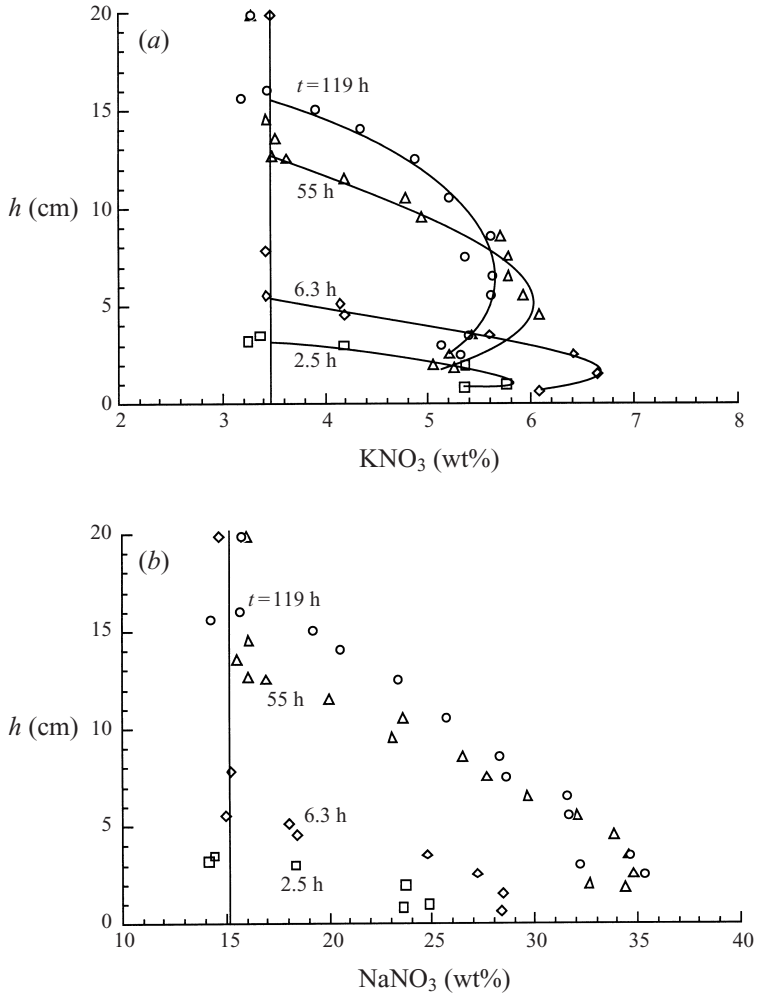


FIGURE 9. The concentrations of (*a*) KNO_3 and (*b*) $NaNO_3$ in the residual liquid as functions of height at various times, as indicated. The vertical lines are the initial concentrations.

cold boundary. It is therefore little affected by the state of the liquid layer. The long initial transient (between 3 h and 10 h) in the growth of the eutectic layer and the long delay in its formation after the base temperature has fallen below the eutectic temperature (at 7 min) may indicate slow nucleation and kinetic growth rates for $NaNO_3$ growing into the interstices of the cotectic mushy layer. We see from figure 8(*b*) that the growth of the eutectic layer is initially linear from a nucleation time of about 2.8 h and with a slope of 4.2×10^{-5} cm s^{-1}. The position of the top of the cotectic mushy layer h_C could not be visualized but was inferred from the measurements of concentration, as described below.

4.4. *Concentration measurements*

Graphs of the concentrations of KNO_3 and $NaNO_3$ in the residual liquid measured in experiment 7 are shown as functions of depth at various times in figure 9. Although there is some scatter in the data, figure 9(*a*) clearly shows turning points (maxima) in the concentration of KNO_3 with height. The maximum concentrations lie in the range

https://doi.org/10.1017/S0022112000003232 Published online by Cambridge University Press

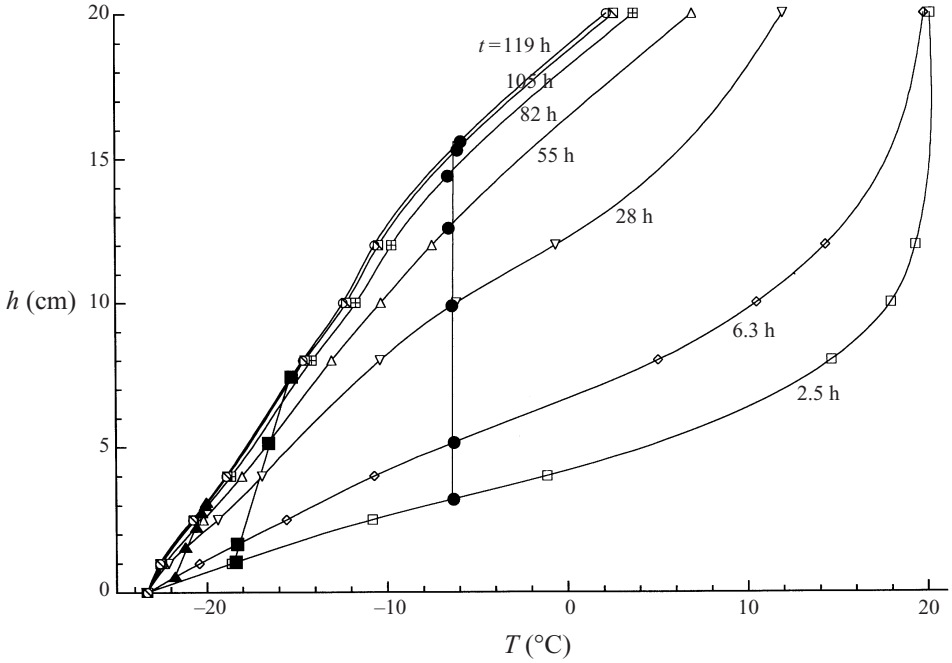


FIGURE 10. Temperature profiles measured at various times during experiment 7. Overlain are the positions of the mush–liquid interface ●, the cotectic front ■ and the eutectic front ▲.

5.5–6.6 wt%. This is a little below the value (6.7 wt%) at which the tie line in the ice field from the initial conditions intersects the simple estimate of the position of the cotectic line shown in figure 4. We shall see later that the liquid lines of descent for all our experiments follow paths below the estimated straight-line cotectic, suggesting that the true cotectic is indeed at lower concentrations of KNO_3. The point at which the tie line meets the cotectic that we estimate later (figure 12) corresponds to a concentration of about 6.0 wt% KNO_3.

The vertical position of the maximum in KNO_3 concentration marks the location of the top of the cotectic mushy layer, below which crystals of KNO_3 are formed in addition to ice. These positions are marked on figure 8(*a*), where we see that the height of the cotectic mushy layer is also approximately proportional to $t^{1/2}$.

There is no obvious turning point, given the scatter in the data, in the concentrations of $NaNO_3$ with height shown in figure 9(*b*). Indeed according to the phase diagram the line of descent along the ice tie line to the H_2O–KNO_3 cotectic and then along the cotectic to the eutectic point should have the concentration of $NaNO_3$ in the residual liquid increasing monotonically.

4.5. *Internal thermal disequilibrium*

Temperature profiles through the lower part of the system, including the solid and mushy regions, are shown for various times in figure 10. These are constructed by interpolating the measurements from the fixed thermistors (at known heights). By using the heights of the various interfaces determined in §§ 4.3 and 4.4, we have superimposed the positions of the interfaces onto the temperature profiles in figure 10 and thereby determined the interfacial temperatures. We see that the mush–liquid interface has an approximately constant temperature of −6.3 °C whereas the

https://doi.org/10.1017/S0022112000003232 Published online by Cambridge University Press

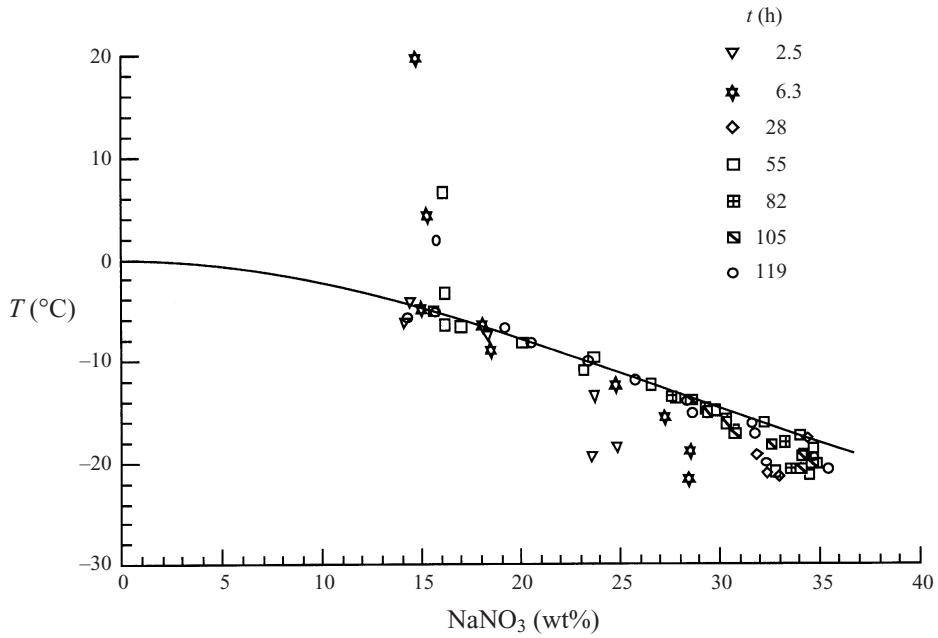


FIGURE 11. Temperature and concentration of $NaNO_3$ in the residual liquid for data from experiment 7. The hand-drawn curve is an indication of the section through the liquidus surface along the tie line and then along the cotectic. The discontinuity in slope between these two sections occurs at about 25.5 wt% $NaNO_3$.

temperatures of the other two interfaces increase with time. This is consistent with the view that the mush–liquid interface has a temperature close to the equilibrium liquidus temperature whereas the other two interfaces are supercooled. The degree of supercooling, if caused kinetically, is expected to decrease (i.e. the temperature is expected to increase) as the rate of solidification decreases (Kirkpatrick, Robinson & Hays 1976; Kerr *et al.* 1990; Worster & Kerr 1994). Indeed the inferred temperatures of the eutectic front are all below the eutectic temperature of $-19.0\,^{\circ}C$.

Further evidence of internal disequilibrium is seen in figure 11, where the temperature is plotted as a function of the concentration of $NaNO_3$ in the residual liquid. The concentration is roughly constant (at its initial value of 15 wt%) in the liquid region and, if equilibrium prevailed, would be expected to follow a path on the liquidus. While this is seen to be approximately true, as indicated by the hand-drawn liquidus through the bulk of the data, the temperature in the lower parts of the mushy layers is seen to fall significantly below the liquidus at early times.

4.6. *The phase diagrams and descent paths*

In figure 12, possibly the most important figure of the paper, we have plotted the KNO_3 and $NaNO_3$ concentrations of the residual liquid taken at various times and locations in all the experiments. Within any particular experiment, these data should, in equilibrium, follow a descent path similar to that depicted in figure 2, i.e. along a tie line and then along a cotectic. The data evolve along the descent path as time increases at a fixed location and as fluid is sampled closer to the cooled boundary at a fixed time. The times and spatial locations are not indicated on the figure. However, all the data collapse onto the respective tie lines for the given initial conditions and

https://doi.org/10.1017/S0022112000003232 Published online by Cambridge University Press

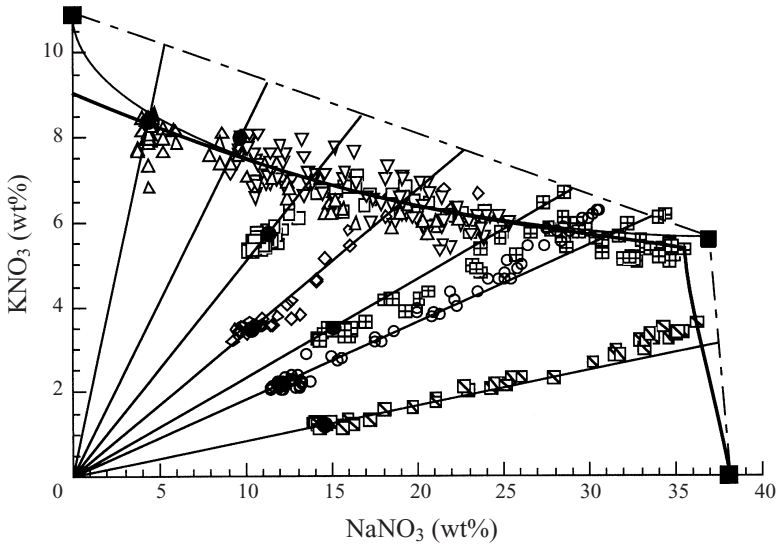


FIGURE 12. Concentration data from the experiments plotted on the ternary phase diagram. The lines from the origin show the tie lines through the initial concentrations. The thin curve is an estimate through the data, tied to the published values of E and E_{AB}, of the cotectic curve. The thicker curve is a new estimate of the cotectics between H_2O and KNO_3 and between H_2O and $NaNO_3$. The latter is more approximate since there is much less data along it. The dot-dashed lines are the original straight-line estimates of the cotectics.

onto a single curve, which can be interpreted as the cotectic between H_2O and KNO_3. No reliable data were collected along the cotectic between H_2O and $NaNO_3$.

We see that all the data lie below the straight line between the binary eutectic point and the three-phase eutectic, shown here with a dot-dashed line (see also figure 4). A hand-drawn curve through our data is shown by the thick line, while the thinner line shows a hand-drawn curve that is constrained to pass through the published binary and ternary eutectic points. These represent new estimates of the cotectic between H_2O and KNO_3. It should be noted that internal disequilibrium as described in § 4.5 would cause the data evolving along the tie line to overshoot the equilibrium cotectic, so we are confident that the true cotectic does indeed lie below the straight line joining the eutectic points.

5. Discussion

We have conducted a series of experiments cooling and crystallizing ternary, aqueous solutions of potassium nitrate and sodium nitrate from below. In each experiment the initial concentration was in the ice field and the density of the residual liquid was such that there was no convection in the system. The height of the ice mushy layer, the cotectic mushy layer of ice and potassium nitrate crystals and the eutectic layer have all been shown to scale with the square root of time, though there was a significant nucleation delay and kinetically limited early growth of the eutectic layer.

These experiments form a baseline against which to assess the role of various modes of thermal and compositional convection that will occur when a ternary melt is cooled and solidified from an upper or lateral boundary or when the initial concentration is such that the residual liquid is buoyant. They also provide quantitative information that can be used in the development and testing of theoretical models of ternary

https://doi.org/10.1017/S0022112000003232 Published online by Cambridge University Press

solidification. Perhaps most importantly, by plotting the concentration of the residual liquid at many different locations and times we have mapped out features of the ternary phase diagram of H_2O–KNO_3–$NaNO_3$ in the ice field, including a new estimate for the cotectic between ice and potassium nitrate. This latter feature, in particular, will aid interpretations of experiments conducted in the KNO_3 field, which we plan to present in the future.

We are very grateful to Mark Hallworth for his help in setting up the experiments, to Ross Kerr for useful comments on the manuscript, and to various members of the Earth Sciences Department for assistance with the atomic absorption measurements. A. A. had a Daphne Jackson Fellowship supported by Lucy Cavendish College, University of Cambridge and the Thriplow Charitable Trust. M. G. W. is supported by the Natural Environment Research Council.

REFERENCES

Huppert, H. E. & Sparks, R. S. J. 1980 The fluid dynamics of a basaltic magma replenished by influx of hot, dense ultrabasic magma. *Contrib. Mineral. Petrol.* **75**, 279–289.

Huppert, H. E. & Worster, M. G. 1985 Dynamic solidification of a binary melt. *Nature* **314**, 703–707.

Huppert, H. E. 1990 The fluid mechanics of solidification. *J. Fluid Mech.* **212**, 209–240.

Kerr, R. C., Woods, A. W., Worster, M. G. & Huppert, H. E. 1990 Solidification of an alloy cooled from above. Part 2. Non-equilibrium interfacial kinetics. *J. Fluid Mech.* **217**, 331–348.

Kirkpatrick, R. J., Robinson, G. R. & Hays, J. F. 1976 Kinetics of crystal growth from silicate melts: anorthite and diopside. *J. Geophys. Res.* **81**, 5715–5720.

Linke, W. F. 1965 *Solubilities of Inorganic and Metal-Organic Compounds*, vol. II, 4th Edn. American Chemical Society.

Mullins, W. W. & Sekerka, R. F. 1964 Stability of a planar interface during solidification of a dilute binary alloy. *J. Appl. Phys.* **35**, 444–451.

Protsenko, P. I., Razumovskaya, O. N. & Brykova, N. A. 1971 Spravochnik po rastvorimosti nitritnykh i nitratnykh solevykh sistem *(Handbook on Solubility of Nitrite and Nitrate Salt Systems)* (ed. A. B. Zdanovski). Leningrad: Khimiya.

Tiller, W. A., Jackson, K. A., Rutter, J. W. & Chalmers, B. 1953 The redistribution of solute atoms during the solidification of metals. *Acta Met.* **1**, 428–437.

West, D. R. F. 1982 *Ternary Equilibrium Diagrams*, 2nd Edn. Chapman and Hall.

Wettlaufer, J. S., Worster, M. G. & Huppert, H. E. 1997 Natural convection during solidification of an alloy from above with application to the evolution of sea ice. *J. Fluid Mech.* **344**, 291–316.

Worster, M. G. 1986 Solidification of an alloy from a cooled boundary. *J. Fluid Mech.* **167**, 481–501.

Worster, M. G. 1992 The dynamics of mushy layers. In *Interactive Dynamics of Convection and Solidification* (ed. S. H. Davis, H. E. Huppert, U. Müller & M. G. Worster). NATO ASI Ser. E, vol. 219, pp. 113–138. Kluwer.

Worster, M. G. 2000 Solidification of fluids. In *Perspectives in Fluid Dynamics* (ed. G. K. Batchelor, H. K. Moffatt & M. G. Worster). Cambridge University Press.

Worster, M. G. & Kerr, R. C. 1994 The transient behaviour of alloys solidified from below prior to the formation of chimneys. *J. Fluid Mech.* **269**, 23–44.

https://doi.org/10.1017/S0022112000003232 Published online by Cambridge University Press